

# Silver-coated TiO<sub>2</sub> nanostructured anode materials for lithium ion batteries

M. M. Rahman · Jia-Zhao Wang · David Wexler ·  
Yu-Yuan Zhang · Xin-Jun Li · Shu-Lei Chou ·  
Hua-Kun Liu

Received: 27 October 2008 / Revised: 6 February 2009 / Accepted: 16 February 2009 / Published online: 3 March 2009  
© The Author(s) 2009. This article is published with open access at Springerlink.com

**Abstract** Anatase TiO<sub>2</sub> nanoribbons/nanotubes (TiO<sub>2</sub>-NRTs) have been synthesised successfully via a reflux method followed by drying in a vacuum oven, and then, silver-coated TiO<sub>2</sub> NRTs (Ag/TiO<sub>2</sub>-NRTs) were prepared by coating silver particles onto the TiO<sub>2</sub>-NRTs surface by the traditional silver mirror reaction. The physical properties of the synthesised products were examined in detail using X-ray diffraction, field emission gun scanning electron microscopy, energy-dispersive X-ray spectroscopy, and transmission electron microscopy, respectively. The results indicated that the Ag nanoparticles were uniformly deposited on the surface of the TiO<sub>2</sub> nanoribbons/nanotubes. The electrochemical properties were investigated by a variety of techniques. The rate capability and cycle durability for the Ag/TiO<sub>2</sub>-NRTs were improved compared with TiO<sub>2</sub>-NRTs. It is speculated that the Ag-coated TiO<sub>2</sub> nanoribbons/nanotubes are an effective anode candidate for lithium ion batteries.

**Keywords** Nanoribbons/nanotubes · Reflux · FEG-SEM · Rate capability · Cycle durability

M. M. Rahman (✉) · J.-Z. Wang · S.-L. Chou · H.-K. Liu  
Institute for Superconducting and Electronic Materials and ARC  
Centre of Excellence for Electromaterials Science,  
University of Wollongong,  
Wollongong, New South Wales, Australia  
e-mail: mmr543@uow.edu.au

D. Wexler  
School of Mechanical, Materials and Mechatronic Engineering,  
University of Wollongong,  
Wollongong, New South Wales, Australia

Y.-Y. Zhang · X.-J. Li  
Guangzhou Institute of Energy Conversion,  
Chinese Academy of Sciences,  
Guangzhou, China

## Introduction

Titanium is the ninth most abundant element in the Earth's crust. Titania (TiO<sub>2</sub>), which is the most common compound of titanium, exists in a number of crystalline forms, the most important of which are anatase and rutile. TiO<sub>2</sub> (anatase) has been extensively studied during the past decade [1]. This interest arises from its potential application in photovoltaic cells [1–3], catalysts [4–6], gas sensing [7], electrochromic devices [8] and rechargeable lithium ion batteries [1, 9–12]. Nanostructured TiO<sub>2</sub> materials, with typical dimensions less than 100 nm, have recently emerged. Such materials include spheroidal nanocrystallites and nanoparticles, together with elongated nanotubes, nanoribbons and nanofibers. Titanium oxide has been found to be one of the best candidates as a lithium ion host because it is a high-capacity material with low cost, non-toxicity and environmental friendliness [13]. Lithium can reversibly be inserted into and extracted from the TiO<sub>2</sub> lattice. The lithium insertion coefficient  $x$  (Li <sub>$x$</sub> TiO<sub>2</sub>) may depend on the crystallography and microstructure of the particular materials. The most active form of TiO<sub>2</sub> for lithium insertion and extraction is anatase, where the reversible insertion coefficient  $x$  is up to 0.5 mol Li per mol TiO<sub>2</sub> [14, 15] at room temperature. A number of methods have been recently reported to prepare one-dimensional nanostructured TiO<sub>2</sub>, such as using porous anodic alumina as a template to obtain TiO<sub>2</sub> nanowires [16] and nanotubes [17, 18], direct anodizing of titanium foil using a hydrofluoric acid aqueous solution as the electrolyte with a platinum plate as the counter electrode [19] and an alkaline hydrothermal approach to convert crystal TiO<sub>2</sub> into nanotubes (nanowires or nanorods) [20, 21]. Amongst these methods, the alkaline hydrothermal approach provides a flexible way to prepare large-scale titanium oxide nano-

tubes to fulfil the requirements for electrode materials. Although the formation mechanism, product structure and composition are still under debate [22–24], the layered nature of the hydrogen titanates seems to be the key to this synthesis process. Until recently, it was believed that such nanotubes and nanowires were composed of TiO<sub>2</sub>-anatase. This hypothesis was called into question by Du et al., and a later work suggested that the nanotubes are composed of the layered titanate H<sub>2</sub>Ti<sub>3</sub>O<sub>7</sub> [25, 26]. Sun and Li have recently confirmed that these nanotubes are indeed titanates, not TiO<sub>2</sub>, and that the as-synthesised materials can be described as Na<sub>x</sub>H<sub>2-x</sub>Ti<sub>3</sub>O<sub>7</sub> ( $x = 0.75$ ) [27]. In addition, Yang et al. produced the formulation Na<sub>2</sub>Ti<sub>2</sub>O<sub>4</sub>(OH)<sub>2</sub> [28]. Armstrong et al. proposed that the as-synthesised nanotubes and nanowires are sodium hydrogen titanates with the general formula Na<sub>y</sub>H<sub>2-y</sub>Ti<sub>n</sub>O<sub>2n+1</sub>·xH<sub>2</sub>O. Acid washing of such materials results in ion exchange to produce the layered hydrogen titanates H<sub>2</sub>Ti<sub>n</sub>O<sub>2n+1</sub>·xH<sub>2</sub>O, which exhibits features similar to H<sub>2</sub>Ti<sub>3</sub>O<sub>7</sub>, H<sub>2</sub>Ti<sub>4</sub>O<sub>9</sub>·H<sub>2</sub>O, and other members of the hydrogen titanate family [11]. The demand for high energy density rechargeable batteries has stimulated the search for new storage electrode materials and the development of new simple methods to prepare old materials.

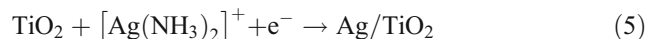
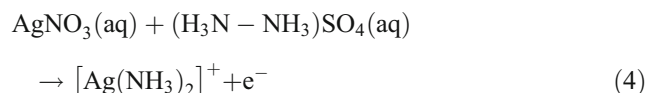
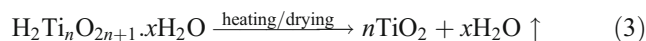
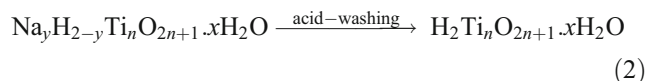
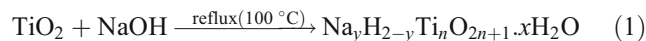
The work presented herein reports on the synthesis via a low temperature (100°C) reflux method of TiO<sub>2</sub> nanoribbons/nanotubes, which were then coated with silver particles by a silver mirror reaction. There are several reports about Ag-modified nanotubes, indeed but no report published to synthesise TiO<sub>2</sub> nanoribbons/nanotubes via reflux method. Most of the reports published about hydrothermal autoclave synthesis at 110–120°C. However, the physical and electrochemical properties of the synthesised products have been investigated in detail. The results revealed that the addition of Ag effectively improved the electronic conductivity, gave a high discharge capacity and improved the cycling stability of the TiO<sub>2</sub> nanoribbons/nanotubes. This method will be a promising one to synthesise nanostructured TiO<sub>2</sub> materials for electronic devices.

## Experimental

### Materials synthesis

Titania nanoribbons/nanotubes were prepared by refluxing anatase TiO<sub>2</sub> powder in a 10 M NaOH solution at 100°C for 12 h. The white precipitate was acid-washed, which involved stirring the sample in 0.1 M HCl solution for 2 h. The material was then filtered, washed with distilled water and dried at 110°C in a vacuum oven for 2 h. Carrying out this reaction at 100°C in a 10 M NaOH solution yields nanoribbons/nanotubes. Washing the products with dilute

HCl promotes complete ion exchange of Na<sup>+</sup> by H<sup>+</sup> to form hydrogen titanates. On drying/heating the products, they convert to anatase TiO<sub>2</sub> nanoribbons/nanotubes. The TiO<sub>2</sub> nanoribbons/nanotubes produced in this way were dispersed into a 0.15 M aqueous silver nitrate solution, and then 0.1 mol/L hydrazine sulfate solution was added dropwise to the suspension under stirring, which reduced the Ag<sup>+</sup> to Ag. The Ag nanoparticles were subsequently deposited onto the surface of the TiO<sub>2</sub> nanoribbons/nanotubes. The possible reactions are as follows:



### Materials characterisation

Powder X-ray diffraction was performed using a Philips 1730 Generator and diffractometer with Cu K $\alpha$  radiation and a graphite monochromator. Traces<sup>TM</sup> software in combination with the Powder Diffraction File (JCPDS) was used to identify the phases present. The morphologies of the products were investigated by scanning electron microscopy (SEM) using either a JEOL 700-1F field emission gun SEM (FEG-SEM) with Bruker energy-dispersive X-ray spectroscopy (EDS) and an X-ray mapping system. Transmission electron microscopy (TEM) investigations were performed using a JEOL 2011 analytical electron microscope. TEM samples were prepared by deposition of ground particles onto lacey carbon support films.

### Electrochemical measurements

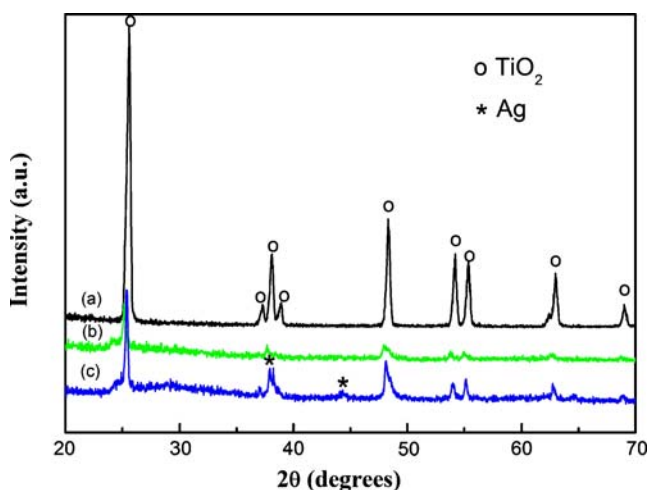
The anode slurry was made by mixing 80% active material with 10% carbon black and 10% polyvinylidene fluoride binder in *N*-methyl-2-pyrrolidinone solvent to form a homogeneous slurry. The slurries were spread onto copper foil substrates. The coated electrodes were dried in a vacuum oven at 100°C for 24 h and then pressed. Subsequently, the electrodes were cut to a 1 × 1 cm<sup>2</sup> size.

CR 2032 coin-type cells were assembled in an Ar-filled glove box (Mbraun, Unilab, Germany) using lithium metal foil as the counter electrode. The electrolyte was 1 M LiPF<sub>6</sub> in a mixture of ethylene carbonate and dimethyl carbonate (1:1 by volume, provided by MERCK KgaA, Germany). The cells were galvanostatically discharged and charged in the range of 1.0–3.0 V at various current densities. AC impedance was measured for the fresh cells at open potential. This was also carried out using the CHI 660C electrochemical workstation system. The AC amplitude was 5 mV, and the frequency range applied was 100 kHz–0.01 Hz.

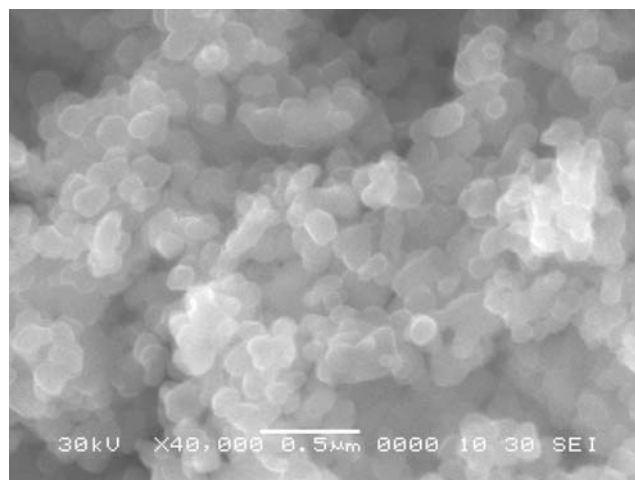
## Results and discussion

Figure 1 presents the X-ray diffraction results obtained from the samples of the raw TiO<sub>2</sub> powder (Raw-TiO<sub>2</sub>), TiO<sub>2</sub> nanoribbons/nanotubes (TiO<sub>2</sub>-NRTs) and Ag-dispersed TiO<sub>2</sub> nanoribbons/nanotubes (Ag/TiO<sub>2</sub>-NRTs). The major peak positions agree with those of the standard TiO<sub>2</sub> anatase phase (JCPDS 84-1285), clearly indicating an anatase based product. The diffraction peaks of the TiO<sub>2</sub>-NRTs are broad, consistent with a nanocrystalline material. The Ag-treated product produced diffraction peaks consistent with the occurrence of a small percentage of crystalline Ag.

Surface morphology, one of the prime factors that govern the physical and electrochemical properties of products, was investigated by means of SEM, FEG-SEM and TEM analysis. SEM imaging (Fig. 2) of the Raw-TiO<sub>2</sub> powder shows the nanoparticle morphology. The particles are spherical agglomerates, which are around 0.5 μm (500 nm) in size.



**Fig. 1** X-ray diffraction results obtained from (a) Raw-TiO<sub>2</sub>, (b) TiO<sub>2</sub>-NRTs and (c) Ag/TiO<sub>2</sub>-NRTs



**Fig. 2** SEM image of Raw-TiO<sub>2</sub> powder

FEG-SEM imaging (Fig. 3a and b) revealed a fibrous product with clumping of fibres into agglomerates. Higher magnification FEM-SEM imaging revealed nanoribbon or nanotube fibrous morphology (Fig. 3a). High-contrast back-scattered imaging (Fig. 3b), combined with X-ray mapping (Fig. 3c), revealed the shape and location of the Ag particles.

Figure 4 shows TEM images of the TiO<sub>2</sub>-NRTs (Fig. 4a) and Ag/TiO<sub>2</sub>-NRTs (Fig. 4b–d) products. For both products, the TiO<sub>2</sub> structure was confirmed by electron diffraction, with the morphology comprising thin ribbons and nanotubes. Preliminary high-resolution imaging (Fig. 4b with diffractogram inset) indicated a high level of defects within the individual ribbons, while the fringe spacing and associated diffractogram in Fig. 4b are consistent with partially disoriented (101) TiO<sub>2</sub> planes. The primary difference between the two products was confirmed by selected area electron diffraction and EDS spot analysis to be the occurrence of relatively large Ag particles (~30–300 nm average diameter), which were randomly dispersed on the outside of the TiO<sub>2</sub>. (The additional Cu peaks and small carbon peaks in the EDS spectra are associated with the Cu support grid and holey carbon support film, respectively.) A tendency of the thin ribbons to roll up into the form of a scroll, giving nanotubes with an approximately circular cross-section, is shown in Fig. 4e and in the FEG-SEM image (Fig. 4f). Further SEM and TEM investigations are required to fully characterise the nanoribbons and nanotubes in terms of crystallography and growth direction.

Figure 5 shows the first, second, tenth and 20th cycle charge–discharge curves for the Raw-TiO<sub>2</sub>, TiO<sub>2</sub>-NRTs and Ag/TiO<sub>2</sub>-NRTs electrodes. The charge–discharge curves for the Raw-TiO<sub>2</sub>, TiO<sub>2</sub>-NRTs and Ag/TiO<sub>2</sub>-NRTs electrodes

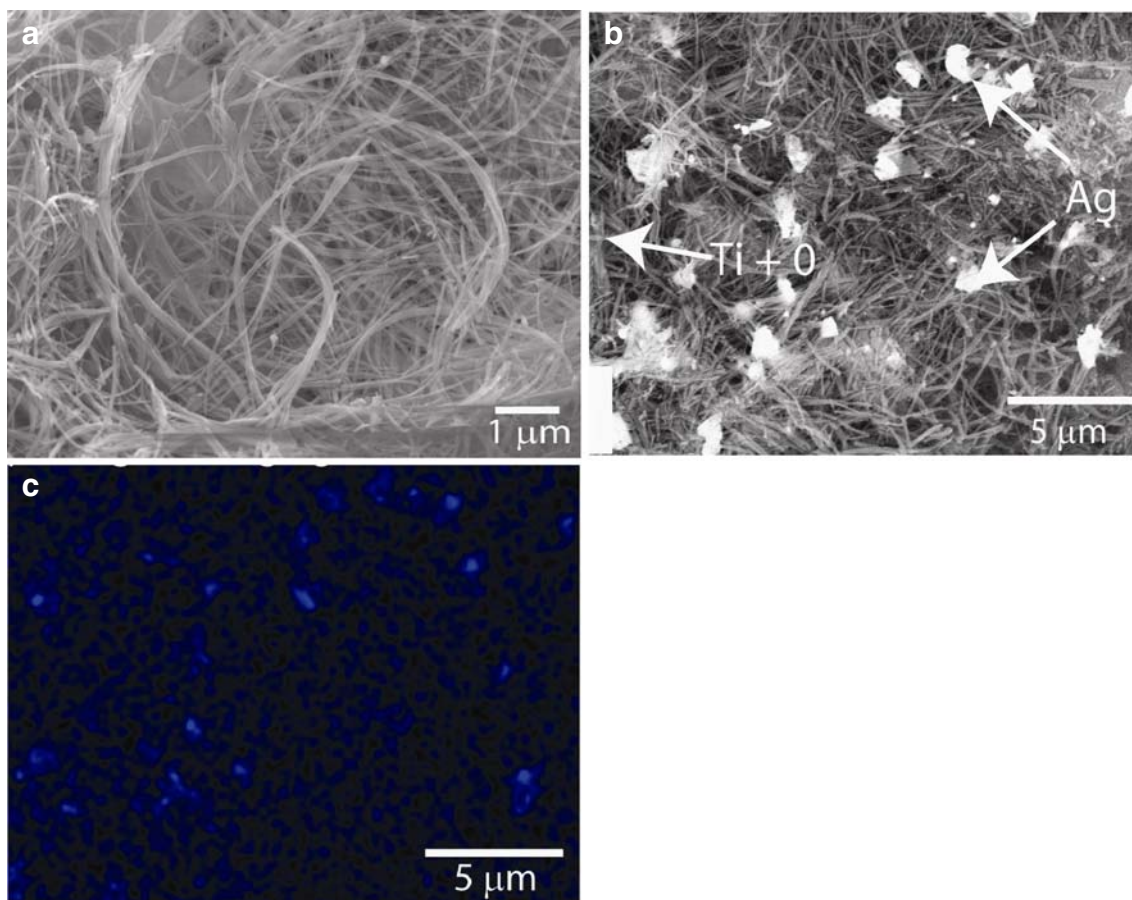


**Fig. 3** Results of FEG-SEM investigation of the Ag/TiO<sub>2</sub>-NRTs product: **a** SE (secondary electron) image, **b** high-contrast BS (back-scattered) image, **c** corresponding X-ray map of Ag for region (**b**)

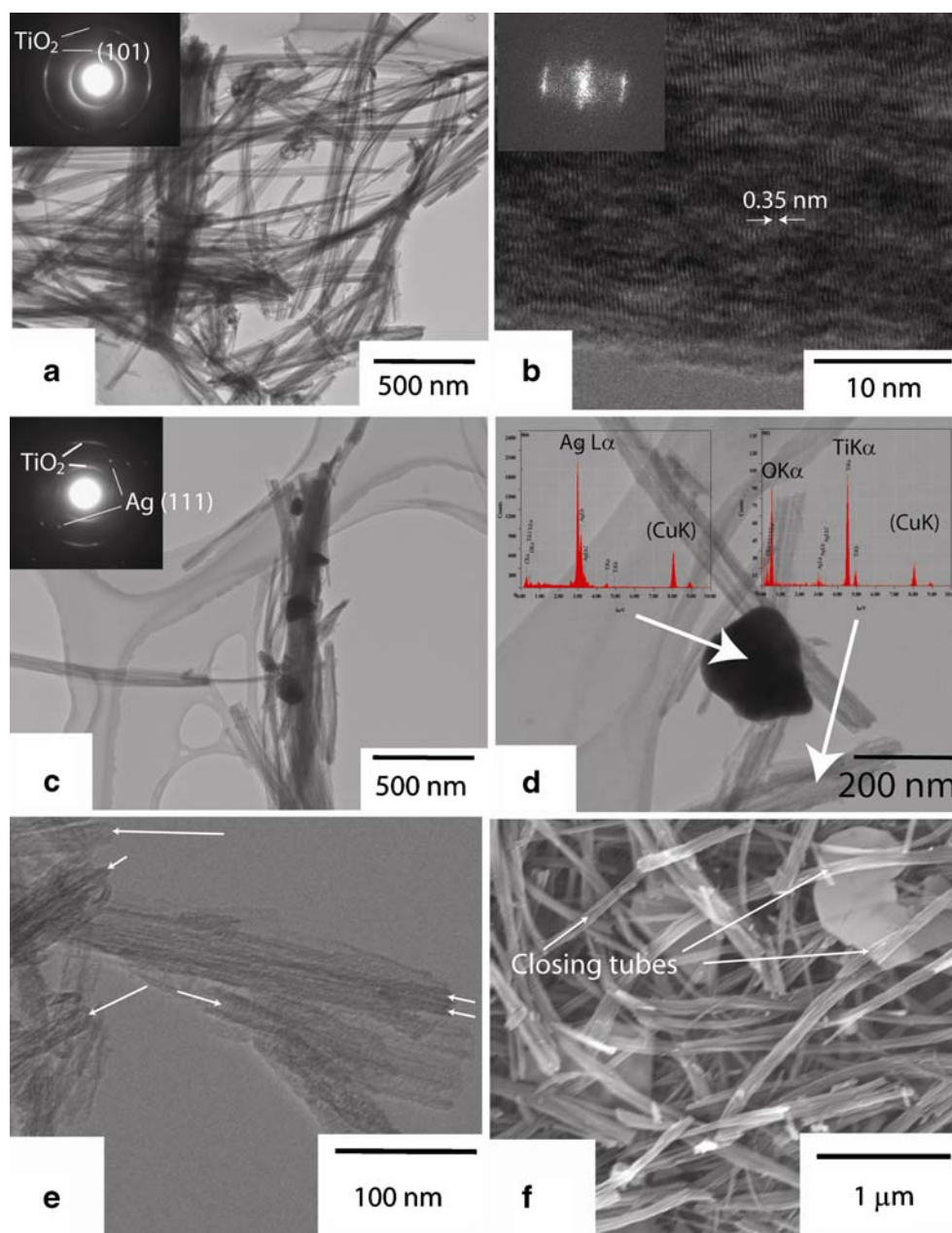
are fairly similar in appearance, but all products show some irreversible capacity losses.

The discharge capacity for the first cycle is higher than the theoretical capacity. The extra capacity could be attributed to the formation of a polymer-like solid–electrolyte interphase (SEI) due to the electrolyte decomposition, corresponding to an irreversible capacity loss in all products. There are distinct potential plateaus observed at 1.75 and 2.06 V for discharging (Li<sup>+</sup> insertion) and charging (Li<sup>+</sup> extraction) for the TiO<sub>2</sub>-NRTs electrode and 1.78 and 2.04 V for discharging (Li<sup>+</sup> insertion) and charging (Li<sup>+</sup> extraction) for the Ag/TiO<sub>2</sub>-NRTs electrode, respectively. Nearly identical potential plateaus have also been reported in the literature [29]. It can be seen in the discharge process that the potential rapidly drops and reaches a plateau of about 1.75 V for the TiO<sub>2</sub>-NRTs electrode and 1.78 V for the Ag/TiO<sub>2</sub>-NRTs electrode and then gradually decreases to 1.0 V in both cases. However, no appreciable change occurs in the voltage profiles over the course of 20 cycles. This behaviour implies that no

observable structural degradation takes place during the lithium extraction/insertion process [30] for the TiO<sub>2</sub>-NRTs and Ag/TiO<sub>2</sub>-NRTs electrodes.

Figure 6 presents the discharge capacity for the Raw-TiO<sub>2</sub>, TiO<sub>2</sub>-NRTs and Ag/TiO<sub>2</sub>-NRTs. The capacities of all products decrease sharply with initial cycling and stabilise after 3 or 4 cycles. After a relatively large capacity drop in the first cycle, the capacity in the fourth cycle was still large, and a favourable cycling capability was present during the subsequent charge/discharge. The initial discharge and charge capacities were measured to be 643.94 and 245.87 mA h g<sup>-1</sup>, 502.79 and 191.25 mA h g<sup>-1</sup> and 380.51 and 206.15 mA h g<sup>-1</sup> for the Raw-TiO<sub>2</sub>, TiO<sub>2</sub>-NRTs and Ag/TiO<sub>2</sub>-NRTs, with a low coulombic efficiency of 38.18%, 38.03% and 54.17%, respectively. This result means that TiO<sub>2</sub> particles/nanotubes can accommodate lithium ions with deep extension initially, and hence, there is a dramatic capacity that will fade during the first several cycles [31]. This process naturally intensifies the rate of electrolyte decomposition and the subsequent SEI forma-

**Fig. 4** TEM images obtained from TiO<sub>2</sub>-NRTs (**a** and **e**) and Ag/TiO<sub>2</sub>-NRTs (**b–d**). The insets contain selected area diffraction patterns (**a** and **c**), while the inset diffractogram corresponding to the lattice image in **b** confirmed the presence of TiO<sub>2</sub> and silver. **d** Bright field image, with the insets containing the results of EDS spot analyses of the regions indicated by arrows. The regions marked by arrows in **e** (TEM image) and **f** (FEG-SEM image) indicate the tendency of nanoribbons to scroll up into nanotubes, with partially open nanotubes clearly visible in the FEG-SEM image



tion. Powders that develop a thick SEI layer often display low ionic conduction, high irreversible capacity loss and poor charge/discharge cyclability. Grugeon et al. reported that the SEI is a translucent film that surrounds the particles (work on CuO). Alternatively, work on Co<sub>3</sub>O<sub>4</sub> has shown that the SEI thickness can be reduced by careful texture control [32].

This suggests that the observed high and sustained irreversible capacity loss up to 3 or 4 cycles for the TiO<sub>2</sub> anodes reported here is due to the SEI formation in all products. The thickness of the SEI will vary between powders due to their different textures. At the 22nd cycle,

the discharge capacities were measured to be 25.58, 154.99 and 184.77 mA h g<sup>-1</sup> for the Raw-TiO<sub>2</sub>, TiO<sub>2</sub>-NRTs and Ag/TiO<sub>2</sub>-NRTs, respectively. The capacity for the Raw-TiO<sub>2</sub> product decreased dramatically, whereas the TiO<sub>2</sub>-NRTs and Ag/TiO<sub>2</sub>-NRTs products showed high discharge capacity, with the Ag/TiO<sub>2</sub>-NRTs product exhibiting superior discharge capacity compared to the TiO<sub>2</sub>-NRTs. The improvement in cycling stability of the cells with nanoribbon/nanotube electrodes, in comparison with the Raw-TiO<sub>2</sub> product, may be due to the following reasons: first, the tube-like structure, which may supply more reactive points for the reaction [33]. Second, the slim

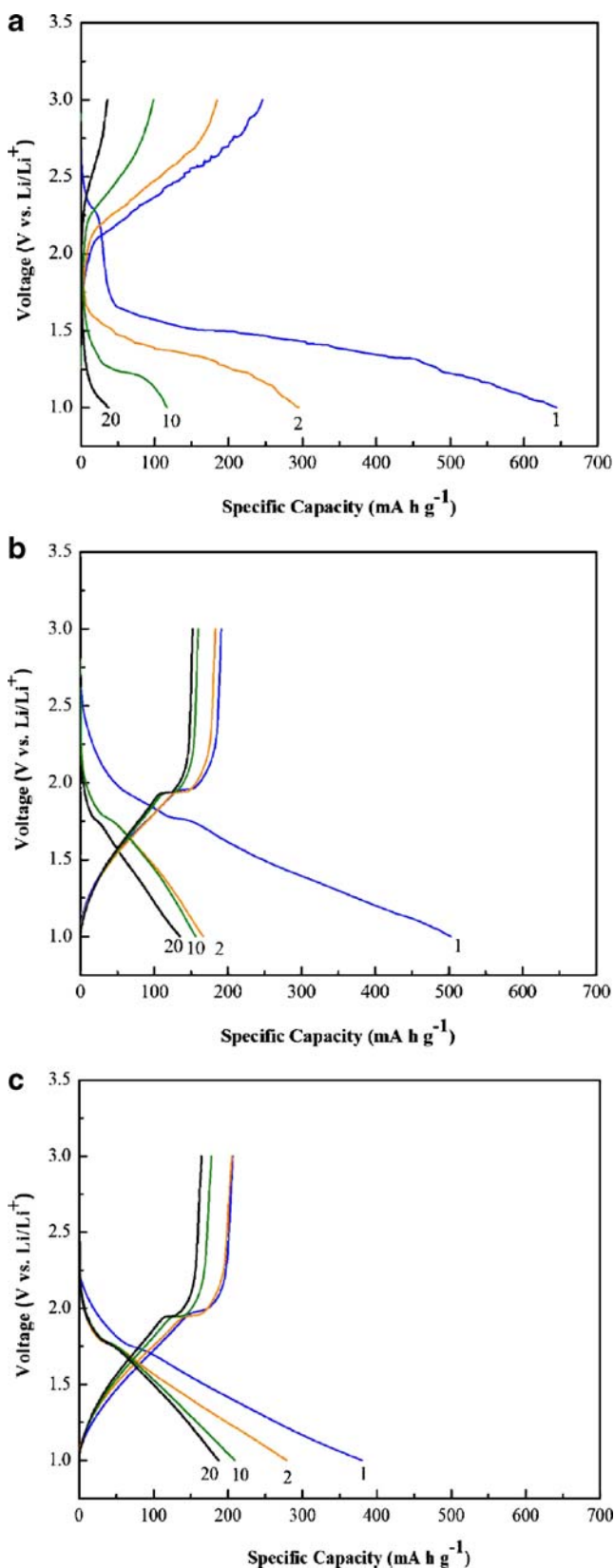


**Fig. 5** Charge–discharge profiles of **a** Raw-TiO<sub>2</sub>, **b** TiO<sub>2</sub>-NRTs and **c** Ag/TiO<sub>2</sub>-NRTs for different cycles under a constant current density of 10 mA g<sup>-1</sup> between 1.0 and 3.0 V

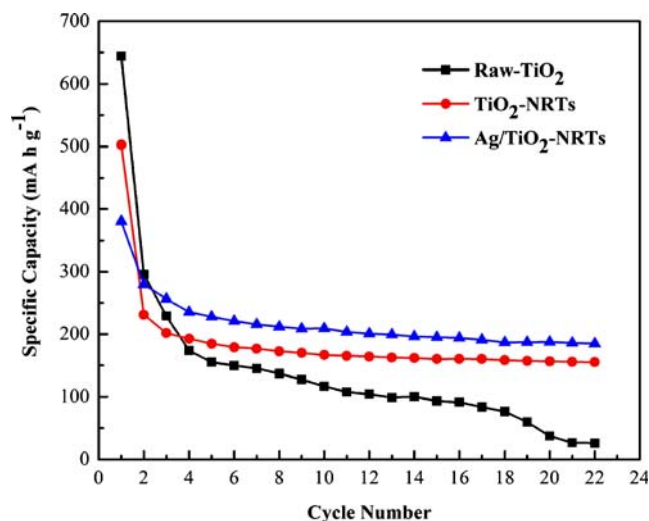


**Fig. 6** Discharge capacities with respect to cycle number for the Raw-TiO<sub>2</sub>, TiO<sub>2</sub>-NRTs and Ag/TiO<sub>2</sub>-NRTs electrodes at 10 mA g<sup>-1</sup>

diameter of the TiO<sub>2</sub> nanoribbons/nanotubes will greatly reduce the distance required for lithium ion diffusion in the solid state [31].

High-rate cycling behaviour is one of the most important electrochemical characteristics of lithium ion batteries, which are required for power storage applications [34]. Cycling performances of the TiO<sub>2</sub>-NRTs and Ag/TiO<sub>2</sub>-NRTs electrodes were thus determined at high current densities. The specific discharge capacity with respect to cycle number for the TiO<sub>2</sub>-NRTs and Ag/TiO<sub>2</sub>-NRTs electrodes at 60 and 120 mA g<sup>-1</sup> is illustrated in Fig. 7. As can be seen, when applying a current density of 60 mA g<sup>-1</sup>, the discharge capacities were measured 154.75 and 210.11 mA h g<sup>-1</sup> at the initial second cycle and 121.05 and 132.73 mA h g<sup>-1</sup> in the 50th cycle for the TiO<sub>2</sub>-NRTs and Ag/TiO<sub>2</sub>-NRTs electrodes, respectively. At 120 mA g<sup>-1</sup>, the discharge capacities were reduced a little to 129.28 and 195.23 mA h g<sup>-1</sup> at the initial second cycle and 83.66 and 102.39 mA h g<sup>-1</sup> in the 50th cycle for the TiO<sub>2</sub>-NRTs and Ag/TiO<sub>2</sub>-NRTs electrodes, respectively, which suggests that the rate capabilities are excellent. It was observed that after several cycles, the charge/discharge processes became very stable, while the coulombic efficiency reached ~100% in the 50th cycle. In addition, it can be seen that the discharge capacities, cycling stability and coulombic efficiency (99.55% at 60 mA g<sup>-1</sup> and 99.11% at 120 mA g<sup>-1</sup>) of the Ag/TiO<sub>2</sub>-NRTs product are higher than those of the TiO<sub>2</sub>-NRTs product (99.24% at 60 mA g<sup>-1</sup> and 99.00% at 120 mA g<sup>-1</sup>) at high current densities. The reason for the better performance with the Ag is because the addition of a conducting metal results in a conducting matrix, which provides a conducting backbone for the tubes, thereby improving the conductivity of the

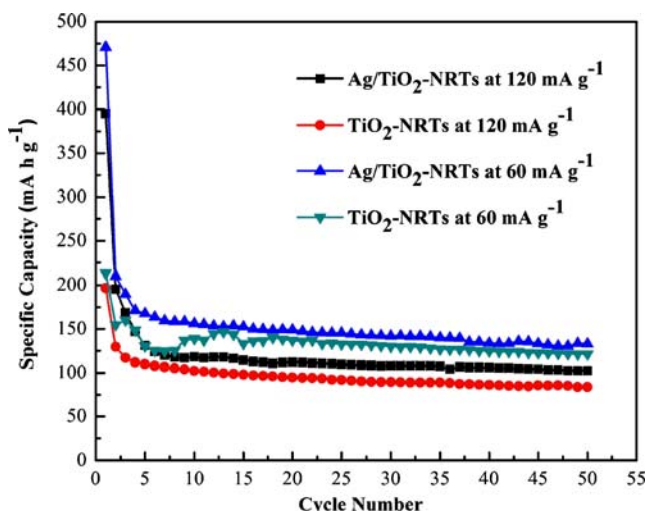


**Fig. 7** Variation of the discharge capacities with respect to cycle number for the TiO<sub>2</sub>-NRTs and Ag/TiO<sub>2</sub>-NRTs electrodes at high current densities (60 and 120 mA g<sup>-1</sup>)

electrode by reducing the tube to tube contact resistance [35], which is confirmed by the results observed in the electrochemical impedance spectroscopy (EIS) analysis.

AC impedance spectroscopy is a powerful technique to determine the kinetic parameters of the electrode process [36, 37], including those in the electrolyte, passivation layers, charge transfer and Li<sup>+</sup> diffusion. AC impedance measurements were performed on the fresh electrodes in order to verify the effect of the silver coating on the electronic conductivity of the Ag/TiO<sub>2</sub>-NRTs electrode. The AC impedance spectroscopy was conducted by applying a sine wave of 0.005 V amplitude over a frequency range of 100 kHz to 0.01 Hz. The Nyquist plots for the TiO<sub>2</sub>-NRTs and Ag/TiO<sub>2</sub>-NRTs electrodes are shown in Fig. 8. All spectra consist of two semicircles at high- and medium-frequency ranges and a line tilted at an approximately 45° angle to the real axis at low frequency.

The AC impedance spectra of the TiO<sub>2</sub>-NRTs and Ag/TiO<sub>2</sub>-NRTs electrodes are modelled by the equivalent circuit. In this equivalent circuit,  $R_s$  is the ohmic resistance of the electrolyte, membrane and electrode, corresponding to the high frequency intercept of the semicircle with the horizontal axis.  $C_{SEI}$  and  $R_{SEI}$  are the capacitance and the resistance of the solid–electrolyte interface layer. This capacitance and resistance are formed due to the reaction between the electrolyte and the surface of the electrode, corresponding to the first semicircle at high frequency region. This high frequency semicircle is assigned to Li migration through surface films at the electrode/electrolyte interface.  $C_{dl}$  and  $R_{ct}$  are the double layer capacitance and the charge transfer resistance, corresponding to the second semicircle at medium frequency. The second semicircle is

attributed to charge transfer kinetics, and the impedance connected with Li transport in the solid phase appears in the low frequency range. Similar results have been reported in literature previously [13]. The sloping line at ~45° to the Z axis found at low frequency is known as the Warburg impedance ( $W$ ) and represents the diffusion of Li ions within the bulk anode/electrode [38]. From the Nyquist plots, it is observed that the semicircle diameter of Ag/TiO<sub>2</sub>-NRTs electrode is shorter than that of TiO<sub>2</sub>-NRTs electrode, implying the charge transfer resistance ( $R_{ct}$ ) of Ag/TiO<sub>2</sub>-NRTs is smaller than that of TiO<sub>2</sub>-NRTs. This result reveals that the transfer rate of Li<sup>+</sup> in Ag/TiO<sub>2</sub>-NRTs is higher than TiO<sub>2</sub>-NRTs, and Ag additive improves the surface electronic conductivity of TiO<sub>2</sub>-NRTs, which makes the transfer of Li ions in TiO<sub>2</sub>-NRTs easier.

### Conclusions

Nanostructured TiO<sub>2</sub>-NRTs were successfully synthesised by the reflux method, and Ag particles were deposited on the surface of the TiO<sub>2</sub>-NRTs using the traditional silver mirror reaction. The electrochemical investigations showed that the Ag/TiO<sub>2</sub>-NRTs electrode presented a higher discharge capacity of 132.73 mA h g<sup>-1</sup> at 60 mA g<sup>-1</sup> and 102.39 mA h g<sup>-1</sup> at 120 mA g<sup>-1</sup> after 50 cycles, good high-rate cycling durability, very high coulombic efficiency (~100%) and superior electrochemical kinetics compared with the TiO<sub>2</sub>-NRTs electrode. The addition of Ag not only decreases the cell polarisation but also increases the transfer rate of Li<sup>+</sup> in TiO<sub>2</sub>-NRTs.

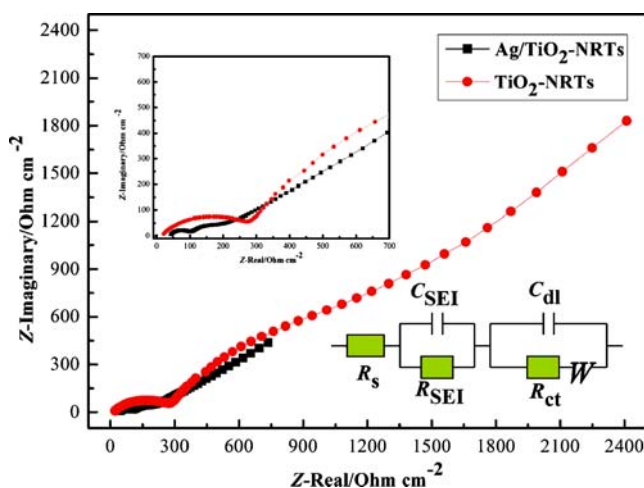


**Fig. 8** Typical electrochemical impedance spectra, presented as Nyquist plots for the TiO<sub>2</sub>-NRTs and Ag/TiO<sub>2</sub>-NRTs electrodes and the equivalent circuit used to fit the EIS

**Acknowledgements** The authors are grateful for funding from the Australian Research Council under an ARC Centre of Excellence Program (CE0561616). The authors also thank Dr. T. Silver for critical reading of the manuscript.

**Open Access** This article is distributed under the terms of the Creative Commons Attribution Noncommercial License which permits any noncommercial use, distribution, and reproduction in any medium, provided the original author(s) and source are credited.

## References

1. Marnix W, Van de Roel K, Arno PMK, Van Well AA, Fokko MM (2001) *J Am Chem Soc* 123:1454
2. Cao F, Oskam G, Searson PC, Stipkala JM, Heimer TA, Farzad F, Meyer GJ (1995) *J Phys Chem* 99:11974. doi:10.1021/j100031a027
3. Hagfeldt A, Gratzel M (1995) *Chem Rev* 95:49. doi:10.1021/cr00033a003
4. Hoffmann MR, Martin ST, Choi W, Bahnemann DW (1995) *Chem Rev* 95:69. doi:10.1021/cr00033a004
5. Anpo M, Takeuchi M (2003) *J Catal* 216:505. doi:10.1016/S0021-9517(02) 00104-5
6. Li D, Haneda H, Hishita S, Ohashi N (2005) *Chem Mater* 17:2596. doi:10.1021/cm049099p
7. Lei Y, Zhang LD, Fan JC (2001) *Chem Phys Lett* 338:231. doi:10.1016/S0009-2614(01) 00263-9
8. Hagfeldt A, Vlachopoulos N, Gratzel M (1994) *J Electrochem Soc* 141:L82. doi:10.1149/1.2055045
9. Huang SY, Kavan L, Gratzel M, Exnar I (1995) *J Electrochem Soc* 142:142. doi:10.1149/1.2048726
10. Ohzuku T, Kodama T, Hirai T (1985) *J Power Sources* 14:153. doi:10.1016/0378-7753(85) 88026-5
11. Armstrong AR, Armstrong G, Canales J, Bruce PG (2004) *Angew Chem Int Ed* 43:2286. doi:10.1002/anie.200353571
12. Kuhn A, Amandi R, Garcia-Alvarado F (2001) *J Power Sources* 92:221. doi:10.1016/S0378-7753(00) 00530-9
13. He BL, Dong B, Li HL (2007) *Electrochem Commun* 9:425. doi:10.1016/j.elecom.2006.10.008
14. Lindstrom H, Sodergren S, Solbrand A, Rensmo H, Hjelm J, Hagfeldt A, Lindquist SE SE (1997) *J Phys Chem B* 101:7717. doi:10.1021/jp970490q
15. Koudriachova MV, Harrison NM, De Leeuw SW (2001) *Phys Rev Lett* 86:1275. doi:10.1103/PhysRevLett.86.1275
16. Zhanag M, Bando Y, Wada K (2001) *J Mater Sci Lett* 20:167. doi:10.1023/A:1006739713220
17. Hoyer P (1996) *Langmuir* 12:1411. doi:10.1021/la9507803
18. Lakshmi BB, Dorhout PK, Martin CR (1997) *Chem Mater* 9:857. doi:10.1021/cm9605577
19. Varghese OK, Gong D, Paulose M, Ong KG, Dickey EC, Grimes CA (2003) *Adv Mater* 15:624. doi:10.1002/adma.200304586
20. Kasuga T, Hiramatsu M, Hoson A, Sekino T, Niihara K (1999) *Adv Mater* 15:1307. doi:10.1002/(SICI) 1521-4095(199910) 11:15<AID-ADMA1307>&t;3.0.CO;2-H
21. Du GH, Chen Q, Han PD, Yu Y, Peng LM (2003) *Phys Rev B* 67:035323. doi:10.1103/PhysRevB.67.035323
22. Yao BD, Chan YF, Zhang XY, Zhang WF, Yang ZY, Wang N (2003) *Appl Phys Lett* 82:281. doi:10.1063/1.1537518
23. Ma R, Bando Y, Sasaki T (2003) *Chem Phys Lett* 380:577. doi:10.1016/j.cplett.2003.09.069
24. Zhang S, Peng LM, Chen Q, Du GH, Dawson G, Zhou WZ (2003) *Phys Rev Lett* 91:256103. doi:10.1103/PhysRevLett.91.256103
25. Du GH, Chen Q, Che RC, Yuan ZY, Peng LM (2001) *Appl Phys Lett* 22:3702. doi:10.1063/1.1423403
26. Chen Q, Zhou W, Du G, Peng LM (2002) *Adv Mater* 14:1208. doi:10.1002/1521-4095(20020903) 14:17<AID-ADMA1208>&t;3.0.CO;2-0
27. Sun X, Li Y (2003) *Chem Eur J* 9:2229. doi:10.1002/chem.200204394
28. Yang J, Jin Z, Wang X, Li W, Zhang J, Zhang S, Guo X, Zhang Z (2003) *Dalton Trans* 3898. doi:10.1039/b305585j
29. Xu J, Jia C, Cao B, Zhang WF (2007) *Electrochim Acta* 52:8044. doi:10.1016/j.electacta.2007.06.077
30. Oh SW, Park SH, Sun YK (2006) *J Power Sources* 161:1314. doi:10.1016/j.jpowsour.2006.05.050
31. Li J, Tang Z, Zhang Z (2005) *Electrochem Solid-State Lett* 8(6): A316. doi:10.1149/1.1904465
32. Grugeon S, Laruelle S, Herrer-Urbina R, Dupont L, Poizot P, Tarascon JM (2001) *Electrochem Soc* 148(4):A285. doi:10.1149/1.1353566
33. Wang D, Zhou F, Liu Y, Liu W (2008) *Mater Lett* 62:1819. doi:10.1016/j.matlet.2007.10.011
34. Huang S, Wen Z, Yang X, Gao Z, Xu X (2005) *J Power Sources* 148:72. doi:10.1016/j.jpowsour.2005.02.002
35. Veeraraghavan B, Paul J, Hala B, Popvo B (2007) *J Power Sources* 109:377. doi:10.1016/S0378-7753(02) 00105-2
36. Wang GX, Bradhurst DH, Liu HK, Dou SX (1999) *Solid State Ion* 120:95. doi:10.1016/S0167-2738(98) 00554-2
37. Mohamedi M, Takahashi D, Itoh T, Umeda M, Uchida I (2002) *J Electrochem Soc* 149:A19. doi:10.1149/1.1424285
38. Kim IS, Blomgren GE, Kumta PN (2005) *J Electrochem Soc* 152(1):A248. doi:10.1149/1.1834894